M. Andrä, J. Zhang, A. Bergamaschi, R. Barten, C. Borca, G. Borghi, M. Boscardin, P. Busca, M. Brückner, N. Cartiglia, S. Chiriotti, G.-F. Dalla Betta, R. Dinapoli, P. Fajardo, M. Ferrero, F. Ficorella, E. Fröjdh, D. Greiffenberg, T. Huthwelker, C. Lopez-Cuenca, M. Meyer, D. Mezza, A. Mozzanica, L. Pancheri, G. Paternoster, S. Redford, M. Ruat, C. Ruder, B. Schmitt, X. Shi, V. Sola, D. Thattil, G. Tinti and S. Vetter, **Development of low-energy X-ray detectors using LGAD sensors**, JOURNAL OF SYNCHROTRON RADIATION, Volume 26, Part 4, July 2019, Pages 1226-1237
https://doi.org/10.1107/S1600577519005393

Development of Low Energy X-ray Detectors using LGAD Sensors

Marie Andrä,[a*1] Jiaguo Zhang,[a2] Anna Bergamaschi,[a] Rebecca Barten,[a] Maurizio Boscardin,[b] Camelia Borca,[a] Paolo Busca,[c] Martin Brückner,[a] Nicoló Cartiglia,[d] Sabina Chiriotti,[a] Gian-Franco Dalla Betta,[e] Roberto Dinapoli,[a] Pablo Fajardo,[c] Marco Ferrero,[d] Francesco Ficorella,[b] Erik Fröjdh,[a] Dominic Greiffenberg,[a] Thomas Huthwelker,[a] Carlos Lopez-Cuenca,[a] Davide Mezza,[a] Aldo Mozzanica,[a] Lucio Pancheri,[e] Giovanni Paternoster,[b] Sophie Redford,[a] Marie Ruat,[c] Christian Ruder,[a] Bernd Schmitt,[a] Xintian Shi,[a] Valentina Sola,[d] Dhanya Thattil,[a] Gemma Tinti[a] and Seraphin Vetter[a]

[a]Paul Scherrer Institut, Forschungsstrasse 111, 5232 Villigen PSI, Switzerland, [b]Fondazione Bruno Kessler, Via Sommarive 18, 38123 Trento, Italy, [c]European Synchrotron Radiation Facility, Grenoble, France, [d]INFN Torino, Via Pietro Giuria 1, 10125 Torino, Italy, and [e]University of Trento, Via Sommarive 9, 38123 Trento, Italy. E-mail: marie.andrae@psi.ch

Abstract

[1] Authors contributed equally to this work.
[2] Authors contributed equally to this work.

Recent advances in segmented Low Gain Avalanche Detectors (LGADs) make them interesting for the detection of low energy X-rays photons thanks to their internal gain. LGAD microstrip sensors fabricated by Fondazione Bruno Kessler have been investigated using X-rays with both charge-integrating and single photon-counting readout chips developed at the Paul Scherrer Institut. The charge multiplication occurring in the sensor allows the detection of X-rays with improved Signal-to-Noise Ratio without additional dark counts. The application in the tender X-ray energy range is demonstrated by the detection of the sulphur K_α and K_β lines (2.3 and 2.46 keV) in an energy dispersive fluorescence spectrometer at the Swiss Light Source. Although improvements in the segmentation and in the quantum efficiency at low energy are still necessary, this work paves the way for the development of single photon-counting detectors in the soft X-ray energy range.

1. Introduction

1.1. Motivation

The advent of large area single photon-counting hybrid detectors developed at the Swiss Light Source allowed huge improvements in many hard X-ray imaging techniques e.g. macromolecular crystallography (Henrich, 2009), powder diffraction (Bergamaschi, 2010) and microscopy (Guizar-Sicarios, 2014). More recently, the development of charge-integrating detectors with single photon resolution and large dynamic range promises to extend the range of application of hybrid detectors to XFEL experiments and to improve the performance in high flux synchrotron experiments (Henrich, 2011; Mozzanica, 2016). Nevertheless, many synchrotron experiments are performed in the soft X-ray energy range (Hitchckock, 2015) due to the higher cross section for thin or low interacting samples and to the presence of the K-edges of many light elements useful e.g. in macromolecular crystallography (Liebschner, 2016) and L-edges of 3D transition metals which are relevant to study copper based superconductors or magnetic structures by means of Scanning X-ray Transmission Microscopy (STXM), ptychography or resonant diffraction (Fink, 2013). These applications are often hindered by the detector performance and usually rely on photodiodes (Gullikson, 1996) and CCDs (Müller et al., 2016). Photodiodes provide a large dynamic range, but they have a relatively high noise which results in low sensitivity and they are not position sensitive. This results in long scanning procedures for aligment and loss of possibly interesting information e.g. in STXM experiments. On the other hand, CCDs provide very low noise (Strüder, 2010; Hall et al., 2011) and high spatial resolution, but they can only run at limited frame rates due to the relatively slow readout times, require a fast shutter and deep cooling, have limited dynamic range due to the full-well-capacity and can easily suffer from radiation damage. Lately many developments have tried to overcome these limitations (Denes, 2011). Recently, Complementary Metal-Oxide-Semiconductor (CMOS) monolithic detectors are also being commissioned for soft X-ray applications (Wunderer, 2014). However, these monolithic detectors still have to prove their performance in terms of versatility, robustness and reliability at the level that hybrid detectors provide at higher energies.

Position sensitive hybrid detectors, as opposite to monolithic, are composed of two separate parts: a sensor where the X-rays convert into electric charge and the readout electronics where the signal is processed and eventually stored or digitized. The sensor is a semiconductor material, normally silicon, where X-rays convert to electron-hole pairs with an electron-hole ($e^{-}h$) pair generation energy of 3.6 eV, segmented into strips (1D) or pixels (2D) in order to provide position sensitivity. Each single element is connected independently to its readout channel of the electronics for highly parallelized performance. This interconnection is obtained by means of wire-bonding (for strips) or bump-bonding (for pixels), introducing a non-negligible capacitance at the input of the readout electronics with a consequent increased noise. For this reason, hybrid strip and pixel detectors have traditionally not been used for soft X-rays, which produce a low signal comparable to the noise of the readout electronics.

The noise of a detector is usually defined by the Equivalent Noise Charge (ENC) (Radeka, 1988) i.e. the charge at the detector input needed to create the same noise at the output. This affects the energy resolution and the presence of noise in the final image, and can be converted from electrons into energy by applying the e^-h pair generation energy of the semiconductor material used. In Photon Counting (PC) detectors, a threshold E_t is applied to the comparator integrated in the frontend electronics and a photon is counted only if the signal generated by a photon exceeds it. In case of monochromatic radiation, E_t is normally set to half of the X-ray energy in order to optimize the quantum efficiency of the detector while avoiding multiple counts due to charge sharing (Kraft, 2009). Equivalently, E_t can be applied offline to the analog data readout from Charge Integrating (CI) detectors in order to discriminate the signal from the noise.

The number of noise counts N_n for the same threshold E_t in a given measurement time T depends on the ENC of the detector, but is different for PC and CI detector with the same noise. In the case of a PC detector, N_n depends on both the ENC and the bandwidth of the noise. It can be estimated by considering the rate of positive zero crossings f_n (Bendat, 1958), resulting in:

$$N_n^{PC} = \frac{T \cdot f_n}{2\pi} e^{\frac{-E_t^2}{2\sigma_{ENC}^2}} \tag{1}$$

where f_n depends on the shaping parameters of the frontend electronics and is usually in the range 1–20 MHz. Considering a relatively slow detector with f_n=2 MHz, one would need a threshold higher than $5\sigma_{ENC}$ to have less than 0.1 % noise counts per second (which sums to 1 kcounts in a 1 Mpixel detector). Even with an noise as low as

σ_{ENC}=46 e^{-} as described in Wicek (2015), one obtains a minimum detectable energy higher than 550 $e^{-}\cdot 3.6$ eV$/e^{-}$ $\approx$2 keV. By setting the threshold higher than half of the X-ray energy, PC detectors can be used below this energy slightly comprimising the quantum efficiency, as described in Donath (2013) down to 1.75 keV.

On the other hand, in a CI detector, the noise is sampled at the readout and can increase with the exposure time Δt, due to the leakage current of the sensor and the to the bandwidth of the frontend electronics. However, for CI hybrid detectors it is normally necessary to subdivide long measurement times T >1–10 ms into multiple frames $n_f = T/\Delta t$ with short exposure time Δt.Therefore the number of noise counts N_n during the exposure time T for a CI detector is (Becker, 2012):

dallabe
2018-11-23 18:12:38
delete

dallabe
2018-11-23 18:12:49
Add space

$$N_n^{CI} = \frac{T}{\Delta t}\,\frac{1 - Erf\left(\frac{E_t}{\sqrt{2}\sigma_{ENC}}\right)}{2} \quad (2)$$

Considering an acceptable exposure time $\Delta t \sim$1 ms without challenging cooling requirements, a threshold cut at $5\sigma_{ENC}$ is required to have less than 0.1 % noise counts per second (which sums to 1 kcounts in a 1 Mpixel detector). Low noise CI detectors have been developed with an $ENC \sim 30\ e^{-}$ (Jungmann-Smith, 2016; Cartier, 2016), resulting in single photon resolution at a minimum energy of 300 $e^{-}\cdot 3.6$ eV$/e^{-}$=1.08 keV. This scales of a factor of 2 in case of small pixels in order to allow charge summation to suppress charge sharing (Cartier, 2016).

However, while the minimum value of $E_t = 5\sigma_{ENC}$ defines a corresponding minimum energy that can be detected by PC detectors, CI detectors can also be operated a low energies without single photon resolution. Being f_n about three orders of magnitude higher than $1/\Delta t$, the number of noise counts at the same threshold and noise is much higher for a PC than for a CI detector.

The ENC of state-of-the-art readout electronics needs to be reduced by almost one order of magnitude in order to make soft X-ray energies energies, spanning from the

dallabe
2018-11-23 18:13:01
delete

iron L-edge at 708 eV for magnetic studies down to the carbon K-edge at 250 eV for imaging of biological specimen, accessible to single photon counting detectors. For this reason, an amplification of the signal in the sensor as the one provided by Low Gain Avalanche Detectors (LGAD) would help to reduce the minimum detectable energy. Moreover, the outstanding timing performance of LGAD sensors, originally developed for tracking charged particles with $\sim$10-20 picosecond timing resolution, could also find applications for time resolved soft X-ray applications (Puzic et al., 2010).

1.2. Low Gain Avalanche Detectors

The development of LGAD sensors is based on the concept of the standard Avalanche Photo Diodes (APD) (Lutz, 2007; Tapan, 1997; Pellegrini, 2014; Pellegrini, 2016). The APDs offer a gain from a few tens to hundreds and they can be used for single photon detection in the visible down to the infrared energy range. However, with such a high gain, the noise performance is degraded due to the significant increase of shot-noise caused by the amplified signal as well as by the leakage current, and thus worsen the signal-to-noise ratio. APDs are fabricated only in small arrays with a pitch of hundreds of microns (Johnson, 2009) and provide an extremely high time resolution. In the hard X-ray energy range they usually exploit indirect conversion in a scintillator since full depletion requires very high voltages ($\sim$1000 V) due to the presence of a highly doped region below the junction.

More recently, Silicon Photo Multipliers (SiPMs) have greatly advanced the technology for the fabrication of segmented amplifying devices, with channel densities that can be up to 10^4 mm^{-2}. While an APD is usually operated using a bias voltage such that the amplified signal stays proportional to the detected one, SiPM are specifically designed to operate with a reverse bias voltage well above the breakdown voltage i.e. in Geiger mode. The resulting gain is of the order of 10^6, but with the disadvantage of a high dark count density even in absence of illumination ($10^5 - 10^6$ pulses/s/mm^2) and a non-negligible propability of afterpulsing i.e. detection of a spurious second pulse on single photon arrival (Bhuzan et al., 2003).

dallabe
2018-11-23 18:13:15
----
probability

The LGAD sensors are built-up on a similar technology as APDs and SiPMs but implemented with a lower concentration of dopants at the junction to reduce the gain to 5–20. LGADs amplify the signal induced by charged particles or photons, generate an output signal which is proportional to the deposited energy and result in an improvement on the signal-to-noise ratio.

Charge multiplication, also known as impact ionization, is the most important mechanism during the operation of LGAD sensors. At the $p-n$ junction, due to the presence of additional dopants (typically with a peak concentration of $\sim 10^{16} - 10^{17}$ cm^{-3}), which is significantly higher than the doping concentration of the silicon substrate ($\sim 10^{11} - 10^{12}$ cm^{-3}), a high electric field is built-up at the junction between the two different kind of dopants. Since the electric field is high, usually above 200-300 kV/cm, carriers gain enough energy while travelling through this region to transfer it to electrons through scattering, which can further ionize silicon atoms with electrons released to the conduction band and holes to the valence band, creating new $e^{-} - h$ pairs (Sze, 2007), which can further create $e^{-} - h$ pairs as well, resulting in a cascade effect. As an example, figure 1(a) shows the electron-induced impact ionization process. After traveling a distance of α_n^{-1} on average, the electron undergoes a collision and a new $e^{-} - h$ pair is generated. $\alpha_{n,p}$ is the impact-ionization coefficient for electrons or holes. Since the impact-ionization coefficient of electrons is $\sim$3 times higher than the one of holes, the electron-induced impact ionization is the dominant process in LGAD sensors (Maes, 1990).

dallabe
2018-11-23 18:13:24
----
delete

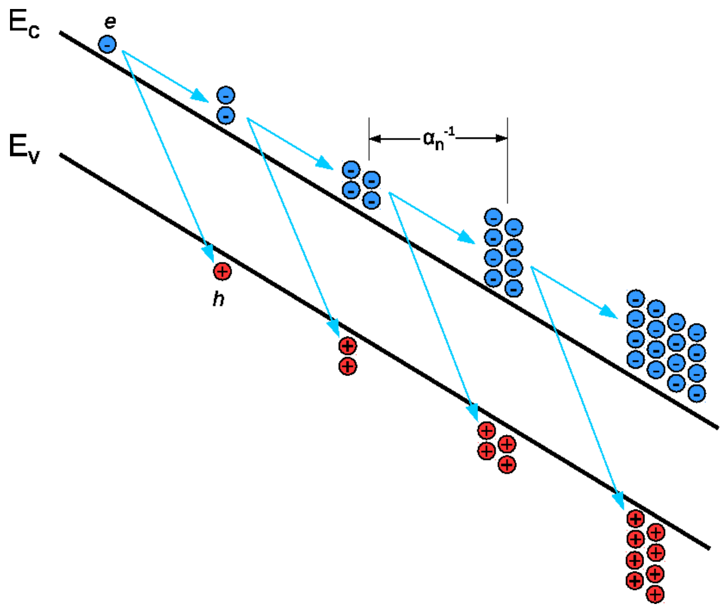

a)

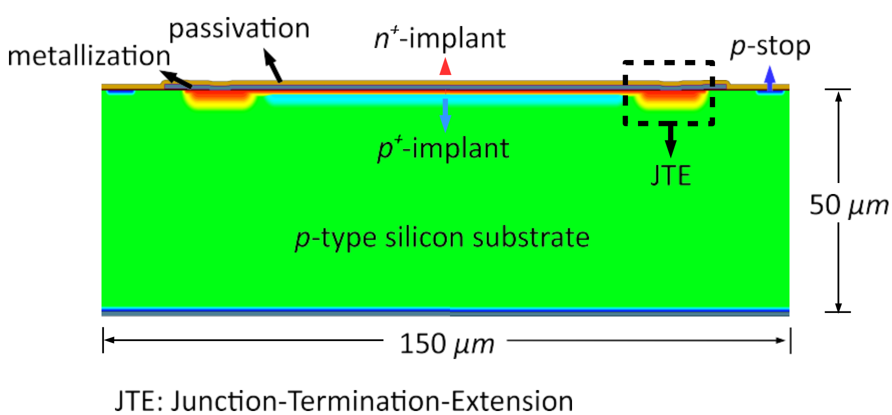

b)

Fig. 1. (a) Conceptual sketch of electron-induced impact ionization. After traveling a distance of α_n^{-1} on average, the electron undergoes a collision with new electron-hole pairs generated by its excess energies. (b) Cross section of the investigated LGAD sensors.

2. Detector description

LGAD microstrip sensors were fabricated by Fondazione Bruno Kessler (FBK, Italy) have been wire-bonded to single photon-counting and charge-integrating readout electronics developed at the Paul Scherrer Institut (PSI, Switzerland) in order to characterize their performance for soft X-ray detection. The LGADs have originally been developed for tracking charged particle with tens of pico-second resolution at the Large Hadron Collider (LHC), while the frontend electronics is optimized for hard X-ray detection using sensors with different geometry and opposite polarity, therefore this work represents a proof of concept rather than a final development for the detection of soft X-rays using hybrid detectors.

dallabe
2018-11-23 18:13:41
----
delete

2.1. The microstrip LGAD sensors

The investigated LGAD sensors are segmented into strips with a pitch of 150 μm and a length of 5 mm. The thickness of the p-type float zone silicon substrate with a resistivity of $\geq$ 5 k$\Omega \cdot cm$ is 50 μm.

The LGADs under investigation are n^{+}-in-p sensors with the n^{+}-side segmented (Paternoster, 2017). The charge multiplication layer is underneath the n^{+}-implant, made by a layer of shallow p^{+}-implant, either Boron or Gallium, whose distribution extends to a few μm below the n^{+} layer. The cross section of a single strip is shown in figure 1(b). A Junction-Termination-Extension (JTE) has been implemented for each strip using deep phosphorous implantation embedding the multiplication layer (Temple, 1997; Fernandez-Martinez, 2016). The design of JTE ensures that no charge multiplication occurs when the $e - h$ pairs generated by charged particles or photons are absorbed in the gap region between two strips, thus the charge multiplication region of each strip is well-defined. The JTE limits the amplification region to the volume below the implant and practically defines a fill factor for the detection of the amplified signal. A *p*-stop has been implemented in order to prevent a short between strips due to the presence of oxide charges after fabrication and X-ray irradiation, which induces an electron-accumulation layer below the SiO_2 layer.

The bulk capacitance of each strip is 1.63 pF from a calculation considering the geometry the LGAD sensor, the interstrip capacitance to the first neighbor is 0.42 pF and 0.05 pF to the second neighbor, with a total capacitive load of 2.57 pF at the input of the frontend electronics. This value is higher compared to the 1.52 pF capacitance measured for the planar silicon microstrip sensors (50 μm pitch, 320 μm thick, 8 mm long) for which the readout electronics used in these experiments were designed (Mozzanica, 2009). Moreover, the settings of the frontend electronics have been optimized for hole collection, while in the case of the LGADs under investigation the signal is negative.

The LGAD sensors were manufactured and handled on top of a 570 μm thick, low resistivity Czochralski wafer, which would absorb all the radiation if irradiated from the backplane. For this reason, all the tests using X-rays have been performed by irradiating the sensor from the strip implant side. The nominal breakdown voltage is found to be $\geq$300 V from the current-voltage (I-V) tests, thus all the X-ray measurements have been done below 300 V.

Two LGAD microstrip sensors with different implantations and doses for the gain layer have been investigated in this study: One with Boron, the other with Gallium. The dose for Boron implantation is about 6% lower than Gallium. Sensors with identical layout as the LGADs but without multiplication layer have also been tested in order to compare the performance of sensors with and without charge multiplication.

2.2. The Mythen-II single photon counting readout

The LGAD strip sensor with Boron implantation using a lower dose (wafer-1) has been wire-bonded to the Mythen-II photon-counting readout chip, which was developed for time-resolved powder diffraction experiments at synchrotron radiation sources. The Mythen-II chip consists of 128 channels operating in parallel (Mozzanica, 2009). Each channel has a charge-sensitive preamplifier that is AC coupled to two shapers followed by a comparator and a 24 bit counter. Only the signals exceeding an externally adjustable threshold are counted and therefore the detector is noise-free for energies above about ten times the electronic noise.

The Mythen-II readout chip is operated in electron collection mode for the LGAD sensors while still using the same standard settings which are normally used for hole collection (Bergamaschi, 2010). The ENC expected for the input capacitance of 2.57 pF corresponding to the LGAD microstrip is about 300 e^{-} RMS ($\sim$1100 eV), which would result in a minimal detectable energy of almost 11 keV compared to $\sim$8.5 keV for standard planar sensors with these settings ($\sim$5 keV with low nise settings (Bergamaschi, 2010)).

dallabe
2018-11-23 18:13:52
noise

2.3. The Gotthard-1.7 charge-integrating readout chip

A different LGAD strip sensor with Gallium implantation using a higher dose (wafer-14) and therefore a higher gain has been wire-bonded to Gotthard-1.7, a charge-integrating prototype readout chip developed for X-ray Free-Electron Lasers (Zhang, 2017; Zhang, 2018). It features a pre-chargeable dynamic gain switching pre-amplifier (PRE) with three gains with increasing feedback capacitance as descirbed in (Mozzanica, 2012) and a fully differential correlated-double-sampling (CDS) stage shared by four readout channels. The PRE output of each channel is connected to a Signal-and-Reset Sampling Stage (SRSS) which consists of two sets of analogue storage cells.

In each set of analogue storage cells, one storage cell is used to record the output of the PRE immediately after reset while the other stores the additional signal induced by the incoming photons. The outputs of the SSRS are multiplexed in group of four channels to one fully differential CDS stage. Signals on the two analogue storage cells are subtracted and amplified by the differential CDS stage so that the CDS differential output is proportional to the integrated charge from the X-ray. Two sets of analogue storage cells are implemented in each channel for dead-time free operation: while one set is connecting to the PRE and storing the output signal from the PRE, the other is disconnected from the PRE and being sampled and processed by the CDS.

3. Measurements

3.1. Leakage current

The leakage current of the LGAD microstrips at different bias voltages has been measured using the Gotthard-1.7 readout chip. Figure 2(a) shows a linear dependence as a function of the integration time for the detector output in absence of radiation at different bias voltages. The leakage current can be estimated by fitting the data with a straight line and converting the angular coefficient into a current using the energy conversion gain g as explained in section 3.2.

The averaged value of the extracted leakage currents for each individual strips as function of bias voltage is shown in figure 2(b). In the voltage range from 60 V to 240 V, the leakage current increases from 0.10 ± 0.01 nA to 0.41 ± 0.04 nA due to the increase of the multiplication factor. For silicon strip sensors without multiplication layer and conventional strip sensors, the leakage currents are 0.02 nA and 0.12 nA respectively, with little dependence on the bias voltage after the sensor is fully depleted. The difference between these sensors is attributed to the different layout design and sensor thickness, as well as the quality of silicon substrate and oxide (e.g. carrier life times and surface recombination velocities). The LGAD sensor shows higher leakage current than both, but it is still in a range which can be handled by the readout chip.

A high leakage current of the sensor results in an increase of the shot noise and therefore a higher electronic noise. Moreover, for CI readout chips, a high leakage current also leads to a reduction of the dynamic range. The Gotthard-1.7 readout chip is optimized for hole collection and has only a limited linear range for the negative polarity (about half of the 14 bit output). A maximum integration time of $\leq$50 μs can be used at bias voltage of 240 V, compared to $\leq$175 μs at 60 V; however, in all cases it is much longer than the 25 μs (at 40 kHz frame rate) readout time of the chip i.e. the detector can be operated in dead-time free mode also using LGADs.

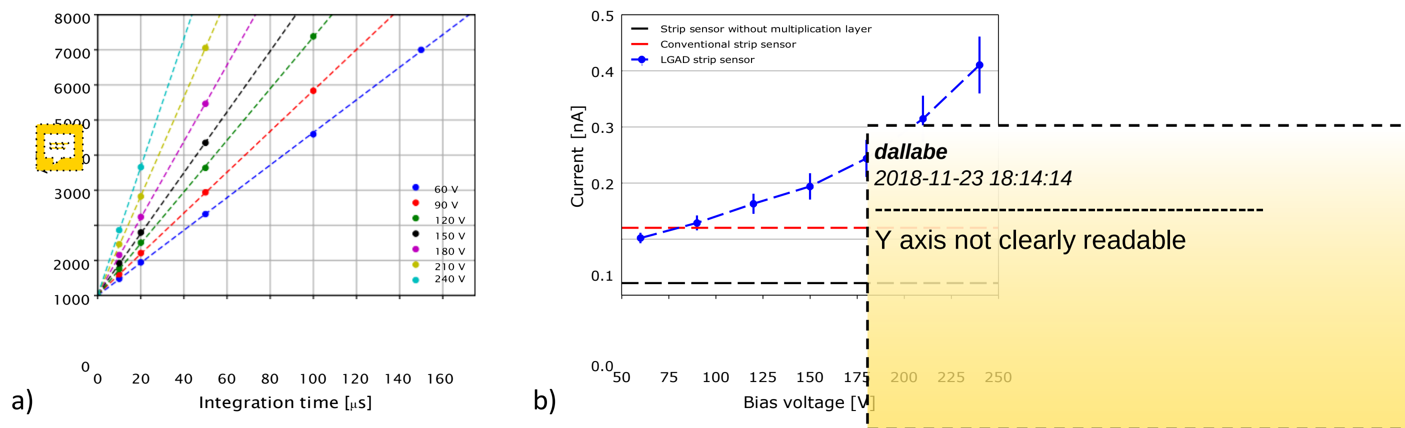

Fig. 2. (a) Dynamic range scan using sensor leakage current for a single strip. (b) Average leakage current over all strips measured using Gotthard-1.7 at different bias voltages compared with sensors without multiplication.

3.2. Energy response

The LGAD strip sensors have been characterized using X-rays emitted by fluorescence targets of different elements excited using the beam generated by an X-ray tube (tungsten or chromium anode). The energy of the detected X-rays is quasimonochromatic with energies ranging between 3.3 keV (Indium L-edge) and 17.5 keV (Molybdenum K-edge).

While the charge-integrating readout of Gotthard-1.7 allows the direct acquisition of a full energy spectrum (pulse height distribution), the energy response of a single photon-counting detector like Mythen-II is obtained by scanning the threshold of the comparator. The resulting curve (S-curve) represents the integral of the spectrum and contains equivalent information. Figure 3 show respectively (a) the spectra acquired with Gotthard-1.7 at 120 V and (b) the S-curves acquired with Mythen-II at 150 V for different X-ray energies, as well as the energy calibration of Gotthard-1.7 and Mythen-II in (c) and (d).

In the case of Gotthard, the energy conversion gain *g* necessary to convert from ADC unit into energy can be estimated by a linear fit of the peak position as a function of the photon energy. For a photon counting detector, the energy conversion is extracted by a linear fit between the position of the inflection point of the S-curves and the photon energy, as described in detail in Bergamaschi (2010).

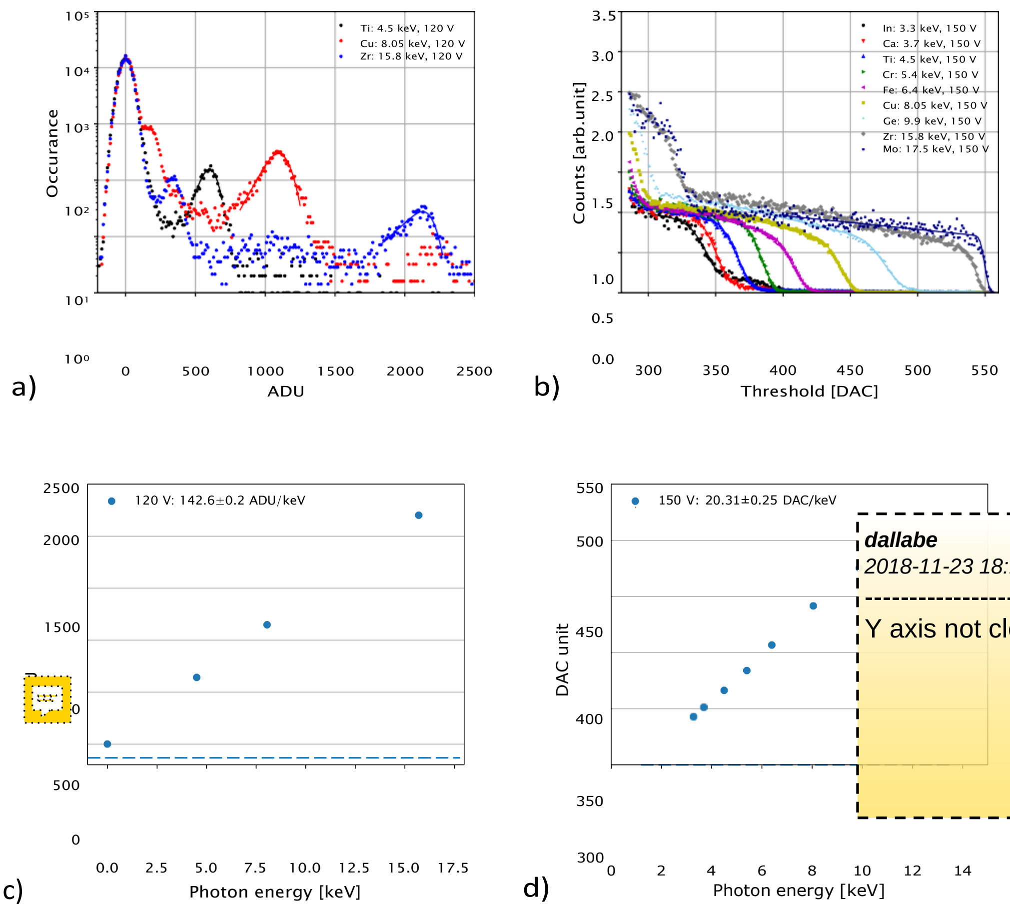

dallabe
2018-11-23 18:14:27
Y axis not clearly readable

Fig. 3. Energy response of the LGAD microstrip sensors at different energies. a) Pulse height distributions acquired using the Gotthard 1.7 chip at 120 V bias voltage. b) S-curves acquired using Mythen-II at 150 V bias voltage. c) Energy calibration using Gotthard-1.7. d) Energy calibration using Mythen-II.

In both cases, for energies above 8.05 keV a shoulder is visible close to the noise level, which is due to X-rays absorbed in the region between the strips and which are not amplified. This signal can be used to estimate the multiplication factor i.e. the ratio between the conversion gain g with and without amplification and the fill factor i.e. the fraction of detected photons whose signal is amplified. Both the multiplication factor and the fill factor depend on the bias voltage applied to the LGADs.

3.3. Multiplication factor

The bias voltage applied to the LGAD sensors modifies the electric field in the multiplication region and therefore affects the signal amplification. Figure 4 shows (a) the pulse height distributions acquired using Gotthard-1.7 and (b) the S-curves acquired using Mythen-II for X-ray fluorescence of 8.05 keV from copper target at different bias voltages. The shift of the peak in the spectra and of the inflection point in the S-curves show an increase of the conversion gain as a function of the applied bias voltage. The increase in the number of counts at higher bias voltages from Mythen-II, as shown in fig 4(b) is probably due to an extension of the amplification region with consequently higher fill factor (see section 3.5).

The multiplication factor, M, of the LGAD sensors is plotted in figure 5 and is estimated from the ratio between the conversion gain of LGAD sensors and planar sensors with the same layout but without multiplication layer. The multiplication factor ranges from 5 to 15 for the voltage range from 60 V to 240 V for the sensor with higher implantation dose and 4 to 6 for the sensor with lower implantation dose. The difference in multiplication factor of the two investigated sensors attributes to the different implantation doses and profiles for the gain layer.

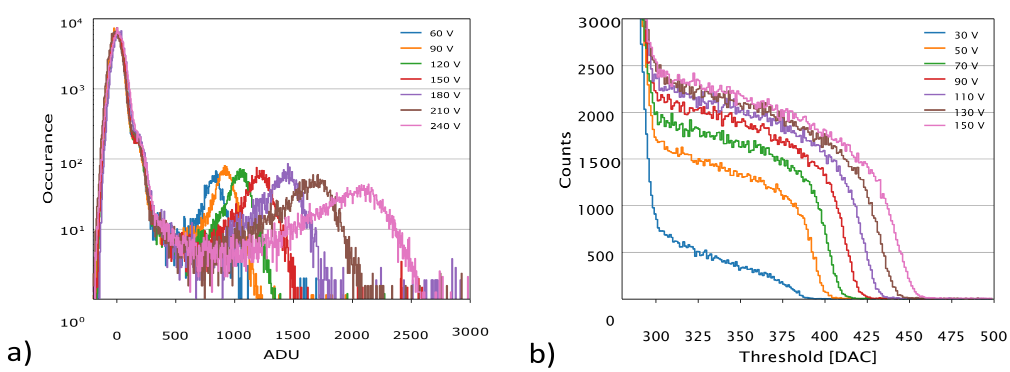

Fig. 4. Response to 8.05 keV copper fluorescence radiation at different bias voltages. a) Pulse height distributions acquired using Gotthard-1.7 and b) S-curves acquired using Mythen-II.

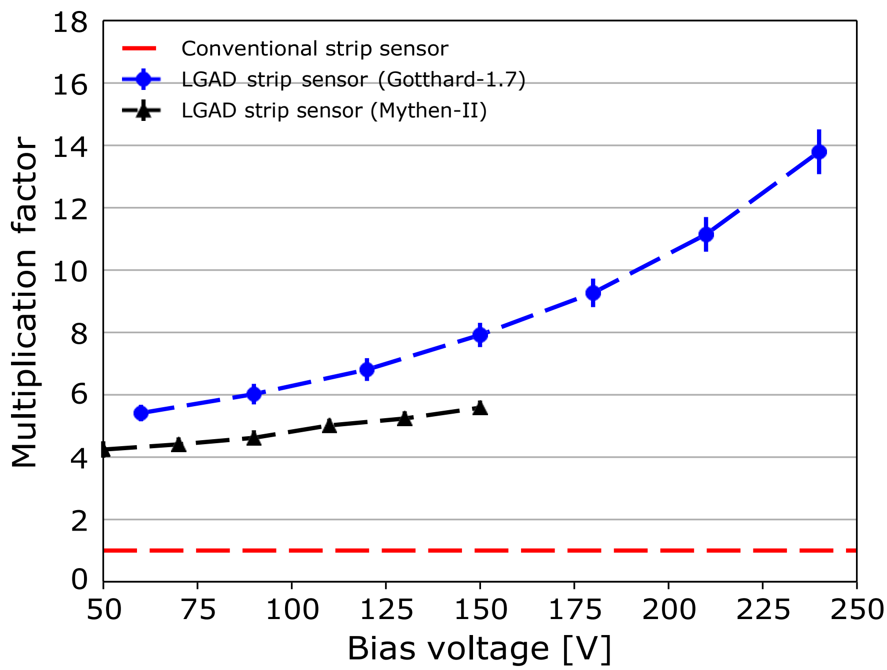

Fig. 5. Average multiplication factor over all strips as function of the bias voltage for the two LGAD strip sensors investigated using Gotthard-1.7 and Mythen-II. The multiplication factors of the two sensors at the same bias voltage are different as they were fabricated using different implants and doses to form the multiplication layer.

3.4. Noise and energy resolution

For Gotthard, the noise has been estimated from the standard deviation of the spectrum in absence of illumination (equivalent to a Gaussian fit to the zero photon distribution), and converted into energy units by using the conversion gain g calculated as in section 3.2). Figure 6(a) shows the noise as function of bias voltage. With increasing bias voltage, the noise in energy decreases since the noise remains constant in electron charge, which is independent of the signal amplification, while the conversion factor g increases.

In addition, the energy resolution has been calculated by fitting the width of the single photon distributions and converting its standard deviation into energy using *g*. The energy resolution *vs.* bias voltage of the LGAD sensor for 8.05 keV X-rays is shown in figure 6(a) as well. It is higher than the noise since it contains both the noise contributions and the variations in the multiplication factor due to the shot noise or to different absorption position. The energy resolution is $\sim 0.41 \pm 0.02$ keV below 180 V. Above 180 V, the pulse height still increases while the shot noise, due to large multiplication, starts to be dominant making the energy resolution at higher bias voltages worse. The best value of energy resolution at 8.05 keV happens at bias voltages of $\leq$ 180 V, corresponding to a multiplication factor of $\sim$10. Compared to the strip sensor without multiplication layer and the conventional strip sensor,the energy resolution has been improved by a factor of 5.5 and 2.7, respectively, in the LGAD sensor.

figure 6(b) shows the energy resolution depends also on the X-[illegible] shows that for low energy X-rays ($\leq$1-2 keV) the energy resolution [illegible] f[illegible] rays i.e. can be improved before the shot noise being dominated for these soft X-rays by increasing the multiplication factor. At 240 V ($M \approx 13.8$), the energy resolution at 1 keV is $\sim$0.21 keV, with a signal-to-noise ratio of about 5, which would enable single photon resolution. An optimized design of the LGAD sensor will improve the energy resolution and further extend the minimal detectable energy, by using sensors with a lower input capacitance compared to the one under test.

dallabe
2018-11-23 18:14:52
dallabe
2018-11-23 18:15:06
----
delete

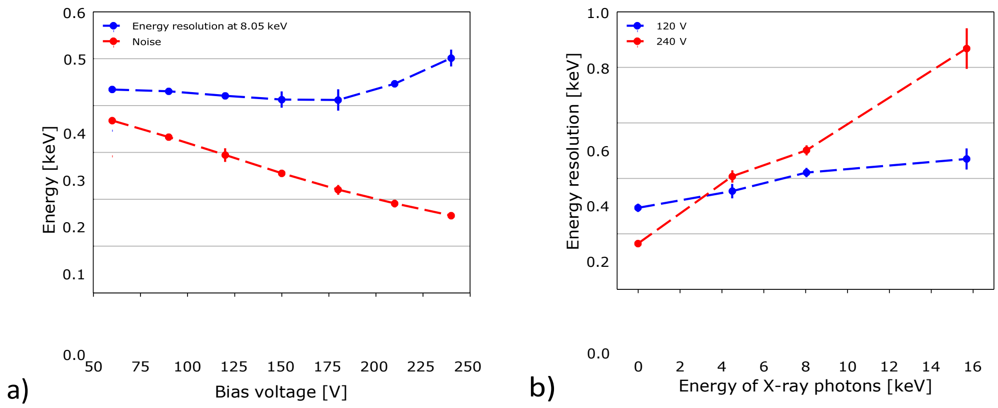

Fig. 6. (a) Average noise over all strip channels as well as energy resolution of 8.05 keV X-rays as function of bias voltage investigated using Gotthard. (b) Energy resolution as function of the photon energy at 120 V and 240 V.

In the case of a single photon-counting detector, the direct measurement of the noise is not possible, while the energy resolution can be estimated by the slope of the S-curve at the inflection point measured using monochromatic radiation (Bergamaschi, 2010). Figure 7 shows the S-curve recorded at the PHOENIX beamline of the Swiss Light Source using 2.1 keV photons for one of the channels of Mythen-II. The strip are illuminated from the front side, i.e. where the gain layer is located.

From the S-curve, a gain of 15.68 DAC/keV is obtained, which is ∼22.80% lower than the gain of 20.31 DAC/keV extracted from the energy calibration shown in figure 3(d) at the same bias voltage of 150 V. This is partially due to the fact that the detector was operated in vacuum and therefore at a higher temperature compared to the measurements in air. Moreover, since the detector is illumintaed from strip side, where the multiplication is located, and the attenuation length of the 2.1 keV photons in silicon is 1.74 μm, most of the photons are absorbed in the gain layer. In this case, the electrons will travel a shorter distance in the gain layer, incurring in less impact-ionization events, with consequent reduced multiplication, while the holes travelling through the gain layer have a lower impact-ionization coefficient.The resulting multiplication coefficienct is therefore lower compared to photons absorbed in the sensor bulk underneath the gain layer. The different absorption depth within the gain layer will also increase the spread of the multiplication factor and therefore degrade the energy resolution.

The average energy resolution for all channels at 2.1 keV is 0.310±0.024 keV RMS. It is reduced of more than a factor of 3 compared to the noise expected for a sensor of the same input capacitance based on hole collection which does not include the variations in the multiplication gain. We expect that this value can be further improved by effectively cooling the detector and by using back-illuminated fully depleted LGADs.

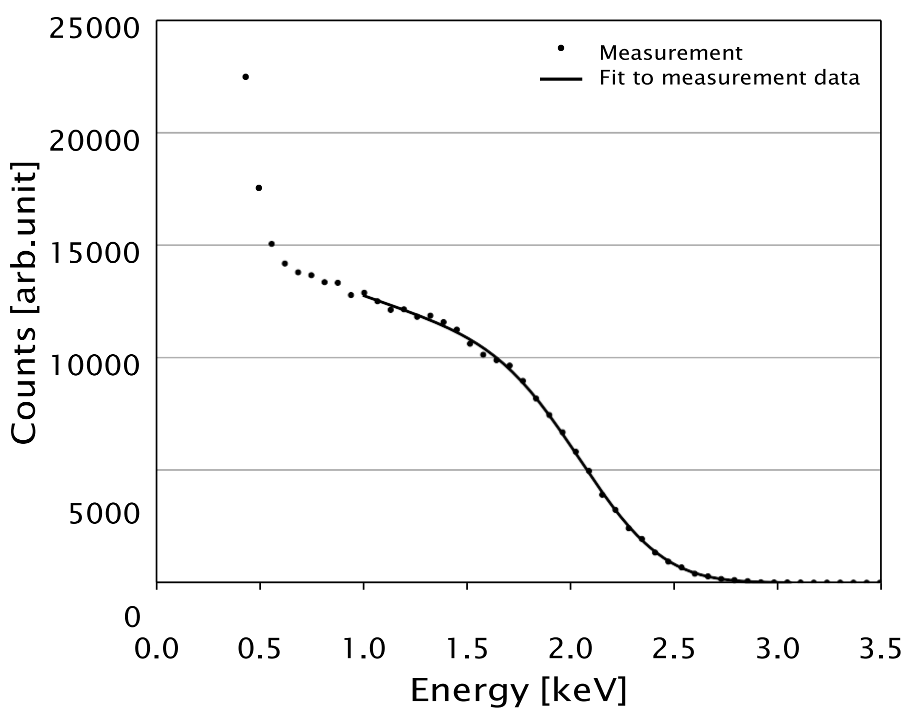

Fig. 7. S-curve of a single strip taken in direct beam of 2.1 keV at the PHOENIX beamline of SLS with a bias voltage of 150 V. The energy resolution estimated from the fit for this channel is 0.310±0.003 keV RMS.

3.5. Fill factor

The JTE limits the multiplication region to the volume below the implant and practically defines a fill factor for the detection of the amplified signal which also depends on the bias voltage. At low energies, the non-amplified X-rays cannot be detected and a low fill factor translates into a reduction of the quantum efficiency.

The S-curves acquired using 17.5 keV photons plotted in figure 8(a) show a second plateau at lower thresholds due to the X-rays absorbed in-between two strips, where no charge multiplication is present in the LGAD sensor. These photons are detected with a signal height like in the planar silicon sensor, while the photons absorbed in the multiplication region are amplified and create a larger signal.

The ratio of the number of counts of the amplified photons and the total number of photons gives the fill factor of the LGADs. Figure 8(b) shows the fill factor measured as a function of the bias voltage. At 50 V it is only 23.6 % at an more than doubles at 150 V (48.0 %) showing that an increase of the electric field can partially improve it.

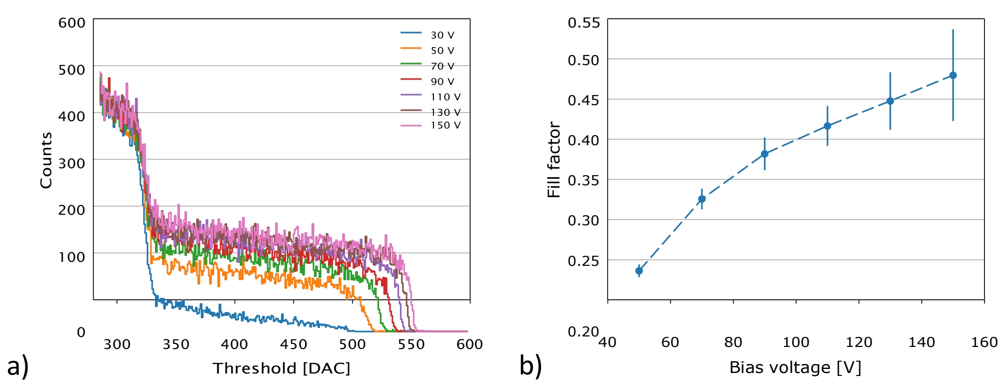

Fig. 8. (a) The S-curves from 17.5 keV X-ray fluorescence at different bias voltages using Mythen-II and (b) determined fill factors of the LGAD sensors at different bias voltages from the S-curves.

To further investigate the position dependence of the multiplication, the LGAD sensor read out using Gotthard was scanned in an X-ray beam of 20 keV focused to ∼3 μm by means of beryllium compound refractive lenses (Snigirev, 1998) at the European Synchrotron Radiation Facility. The sensor was biased to 120 V during the measurement. The measured energy as function of beam position crossing three strips is shown in figure 9(a) and their projection to the *x*-axis in figure 9(b). The region with measured energy above 1 in the figure indicates the region with charge multiplication. The fill factor, defined by the percentage of the area with measured energy higher than 50 % of the maximum in the scan, is $\sim$40 %, corresponding to a width of 60 μm and a gap of 90 μm (without or with lower multiplication). Inside the area with charge multiplication, the mean value of the measured energy varies at different positions indicating a gain variation. From the measurement, it is shown that the non-uniformity of the measured energy due to the gain variation is smaller than the noise.

Figure 9(c) shows the spectrum of one investigated strip when X-rays illuminate different regions: (a) The non-multiplication region (M=1), (b) the transition region with and without multiplication, as well as (c) the multiplication region (M=6.7 at 120 V). The peak at zero ADU is caused by the noise of the system. In (a), up to three single photon peaks, labeled as 1,2,3 ph (M=1), can be seen in the spectrum for the photons without charge multiplication. The photon peaks are at 435 ADU, 870 ADU and 1305 ADU for one, two and three photons, respectively. In (b), both single photons with and without multiplication are visible. The single and double photon peaks at 435 ADU and 870 ADU remain visible, while a third peak at 2500 ADU arises due to the signal multiplication of the single photons. In (c), only photons with charge multiplication can be seen. Here, the single photon peak is located at 2935 ADU and two photons create a signal of 5870 ADU. Note that the ”single” photon peak with charge multiplication in (b) shows slightly lower pulse height at 2500 ADU compared to 2935 ADU for photons absorbed in (c) which has to be attributed to only partial multiplication of the charges due to diffusion of electrons during drifting to the readout electrode driven by the electric field inside the sensor.

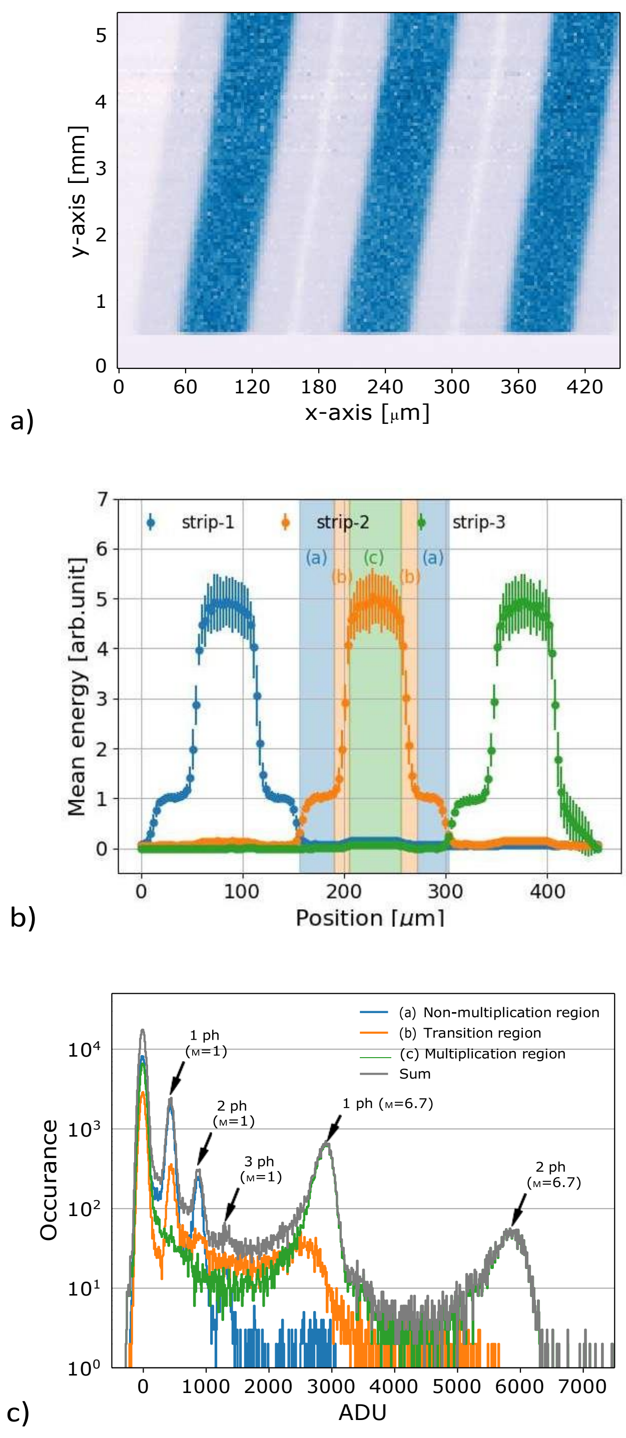

Fig. 9. a) Mean energy measured as a function of the position of the pencil beam on a region of three strips, b) a profile of the image and c) spectrum measured in the different regions. Labels in b) refer to the different regions shown in c).

4. Tender X-ray energy dispersive spectrometer measurements

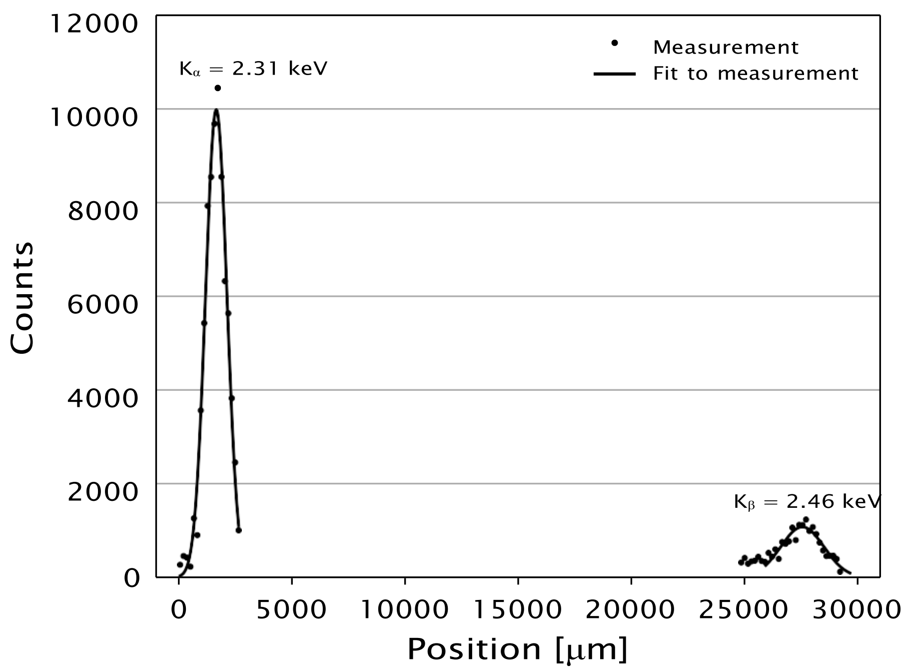

Fig. 10. Fluorescence emission spectrum of Sulfur, taken with a von Hamos spectrometer at the PHOENIX beamline of SLS.

As a proof of principle, the LGAD with the Mythen readout was tested in a von Hamos spectrometer operating in the tender X-ray energy range (2-4 keV) installed at the PHOENIX beamline of the Swiss Light Source (Huthwelker, 2018). The spectrometer normally uses the CI MÖNCH detector (Ramilli, 2017), which provides single photon resolution at these energies. However, the detected flux is very low and a PC readout, as normally used in the hard X-ray energy range, would be more appropriate (Slatcheko, 2012).

Figure 10 shows a fluorescence emission spectrum of Sulfur recorded using an unfocused X-ray beam of 3 keV. The K_α=2.31 keV and K_β=2.46 keV lines are located on two separate sensors assembled on the same module. The fluorescence lines are well detected even without threshold equalization, which is outstanding compared to the minimum detectable energy of about 11 keV for the detector with planar silicon sensors of the same geometry. For the standard sensor the detector limit is 5 keV thanks to the smaller sensor capacitance and optimized settings.

The spectrum has been acquired in a single acquisition with an exposure time of 15 s. In order to acquire the same spectrum using MÖNCH, 15000 frames should have been acquired and analyzed in order to extract the photons, requiring a high performance data backend system.

Still, this measurement is only a proof of principle. The spectrometer would require a spatial resolution of better than 50 μm in order to provide the expected 0.5 eV energy resolution and separate e.g. the $K_{\alpha1}$, $K_{\alpha2}$ doublet using the focused beam. This is clearly not yet achievable with the current sensors due to the large strip pitch and low fill factor and will require further development of the LGAD technology.

5. Discussion

An LGAD strip sensor segmented on the n^+-side has been investigated and results demonstrate the possibility to extend the minimal detectable energy of X-rays for PC and the single photon resolution for CI microstrip detectors down or below 2 keV. These results have been obtained with sensors developed for ultrafast tracking of charged particles, with a high input capacitance and readout electronics with relatively high noise (ca. 300 e^- for Mythen-II and Gotthard-1.7, both optimized for hole collection). Therefore we expect that this minimum energy can be improved down to about 500 eV in order to include the L-edges of 3D transition metals by careful optimization of the LGAD technology and matching of the readout electronics.

Moreover, for most X-ray applications, the segmentation of the sensors should be reduced to at least 100 μm with a fill factor close to 100% in order to improve the spatial resolution and the quantum efficiency. This can be obtained by optimizing the design layout of the JTE, exploting charge diffusion using back illuminated thick silicon sensors or alternatively by developing inverse LGADs with the multiplication layer on the rear side (Paternoster, 2017).

Pixel detectors require back illumination of the sensors, therefore LGADs without substrate and with shallow backplane ($\leq$200 nm implant) must be optimized in order to obtain a high quantum efficiency below 1 keV.

This study represents only a proof of principle for using LGAD sensors for soft X-ray detection. Despite the many technological challenges for improving the capacitance, the leakage current, the segmentation and the quantum efficiency, we expect that the LGAD technology could be a breakthrough for the development of soft X-ray single photon counting detectors, which would be a game changer for several resonant diffraction and spectromicroscopy applications.

Acknowledgements

The tender X-rays synchrotron radiation measurements have been carried out at the PHOENIX beamline of the Swiss Light Sources. The pencil beam scan has been performed at the BM05 beamline of the European Synchrotron Radiation Facility.

References

J. Becker et al., The single photon sensitivity of the adaptive gain integrating pixel detector, *Nucl. Instrum. Methods Phys. Res. A* 694, 82–90 (2012).

S. Bendat, *Principles and Applications of Random Noise Theory*, J. Wiley and Sons, p. 125, (1958).

A. Bergamaschi et al., The MYTHEN detector for X-ray powder diffraction experiments at the Swiss Light Source, *J. Synchrotron Radiat.* 17, 653–668 (2010).

P. Bhuzan et al., *Nucl. Instrum. Methods Phys. Res. A* 504, 48–52 (2003).

S. Cartier et al., Micrometer-resolution imaging using MNCH: towards G2-less grating interferometry, *J. Synchrotron Radiat.* 23, 1462–1473 (2016).

P. Denes et al., Development of a compact fast CCD camera and resonant soft x-ray scattering
475 endstation for time-resolved pump-probe experiments, *Rev. Sci. Instr.* 82, 073303, (2011).

T. Donath et al., Characterization of the PILATUS photon-counting pixel detector for X-ray
476 energies from 1.75 keV to 60 keV, *J. Phys.: Conf. Ser.* 425, 062001, (2013).

P. Fernandez-Martinez et al., Design and fabrication of an optimum peripheral region for low
477 gain avalanche detectors, *Nucl. Instrum. Methods Phys. Res. A* 821, 93–100 (2016).

478 J. Fink et al., Resonant elastic soft x-ray scattering, *Rep. Prog. Phys.* 76, 056502, (2013).

M. Guizar-Sicarios et al., High-throughput ptychography using Eiger: scanning X-ray nano-
479 imaging of extended regions, *Optics Express* 22, 14859–14870, (2014).

E. M. Gullikson et al., Stable silicon photodiodes for absolute intensity measurements in the VUV and soft X-ray regions, *Journal of Electron Spectroscopy and Related Phenomena* 80,
480 313–316 (1996).

D. J. Hall et al., Photon-counting imaging camera for high-resolution X-ray and γ-ray appli-
481 cations, *JINST* 6 C01022, (2011)

B. Henrich et al., PILATUS: A single photon counting pixel detector for X-ray applications,
482 *Nucl. Instrum. Methods Phys. Res. A* 607, 247–249 (2009).

B. Henrich et al., The adaptive gain integrating pixel detector AGIPD a detector for the
483 European XFEL, *Nucl. Instrum. Methods Phys. Res. A* 633, S11–S14 (2011).

A. P. Hitchcock, Soft X-ray spectromicroscopy and ptychography, *Journal of Electron Spec-*
484 *troscopy and Related Phenomena* 200, 49–63 (2015).

T. Huthwelker et al., Von Hamos spectrometer fot the tender X-ray energy range at the
485 PHOENIX beamline, *in preparation* (2018).

J. Jungmann-Smith et al., Towards hybrid pixel detectors for energy-dispersive or soft X-ray
486 photon science, *J. Synchrotron Radiat.* 23, 385 (2016).

P. Kraft et al., Performance of single-photon-counting PILATUS detector modules, *J. Syn-*
487 *chrotron Radiat.* 368, 385 (2009).

D. Liebschner et al., On the influence of crystal size and wavelength on native SAD phasing,
488 *Acta Cryst.* D72, 728–741 (2016).

G. Lutz, *Semiconductor Radiation Detectors, Device Physics*, Springer-Verlag, Berlin Heidel-
489 berg, ISBN:978-3-540-71678-5 (2007).

W. Maes et al., Impact ionization in Silicon: A review and update, *Solid-State Electronics*
490 33(6), 705–718 (1990).

N. Moffat et al., Low Gain Avalanche Detectors (LGAD) for particle physics and synchrotron
491 applications, *J. Instr.* 13, C03014 (2018).

A. Mozzanica et al., MythenII: A 128 channel single photon counting readout chip, *Nucl.*
492 *Instrum. Methods Phys. Res. A* 607, 250–252 (2009).

A. Mozzanica et al., The GOTTHARD charge integrating readout detector: design and char-
493 acterization, *J. Instr.* 7, C01019 (2012).

A. Mozzanica et al., Characterization results of the JUNGFRAU full scale readout ASIC, *J.
494 Instr.* 11, C02047 (2016).

M. Müller et al., Table-top soft X-ray microscopy with a laser-induced plasma source based
495 on a pulsed gas-jet, *AIP Conference Proceedings* 1764, 030003 (2016)

G. Paternoster et al., Developments and first measurements of Ultra-Fast Silicon Detectors
496 produced at FBK, *J. Instrum.* 12, C02077 (2017).

G. Pellegrini et al., Technology developments and first measurements of Low Gain Avalanche Detectors (LGAD) for high energy physics applications, *Nucl. Instrum. Methods Phys. Res.*
497 *A* 765, 12–16 (2014).

G. Pellegrini et al., Recent technological developments on LGAD and iLGAD detectors for
498 tracking and timing applications, *Nucl. Instrum. Methods Phys. Res. A* 831, 24–28 (2016).

A. Puzic, et al., Photon Counting System for Time-resolved Experiments in Multibunch Mode,
499 *Synchrotron Radiation News* 23:2, 26–32 (2010).

M. Ramilli et al., Measurements with MÖNCH, a 25 μm pixel pitch hybrid pixel detector, *J.*
500 *Instr.* 12, C01071 (2017).

J. Szlachetko et al., A von Hamos x-ray spectrometer based on a segmented-type diffraction crystal for single-shot x-ray emission spectroscopy and time-resolved resonant inelastic x-ray
501 scattering studies, *Rev. Sci. Instr.* 83, 103–105 (2012).

A. Snigirev, et al., Focusing high-energy x-rays by compound refractive lenses,*Applied Optics*
502 37, 653-662 (1998).

L. Strüder et al., Large-format, high-speed, X-ray pnCCDs combined with electron and ion imaging spectrometers in a multipurpose chamber for experiments at 4th generation light
503 sources, *Nucl. Instrum. Methods Phys. Res. A* 614(3), 483–496 (2010).

L. Strüder, chapter in *Synchrotron Light Sources and Free Electron Lasers*, Springer Interne-
504 tional Publishing Switzerland, 1059–1088 (2016).

S.M. Sze, *Physics of Semiconductor Devices*, John Wiley & Sons, Inc., Hoboken, New Jersey,
505 ISBN-10:0-471-14323-5 (2007).

I. Tapan et al., Avalanche photodiodes as proportional particle detectors, *Nucl. Instrum.*
506 *Methods Phys. Res. A* 388, 79–90 (1997).

507 A.K. Temple, *1997 International Electron Devices Meeting* 23, 423–426 (1997).

P. Wiacek et al., Position sensitive and energy dispersive x-ray detector based on silicon strip
508 detector technology, *J. Instrum.* 10, P04002 (2015).

509 C. Wunderer et al., The PERCIVAL soft X-ray imager, *J. Instrum.* 9, C03056 (2014).

J. Zhang et al., Performance evaluation of the analogue front-end and ADC prototypes for the
510 Gotthard-II development, *J. Instrum.* 12, C12052 (2017).

J. Zhang et al., Towards Gotthard-II: development of a silicon microstrip detector for the
511 European X-ray Free-Electron Laser, *J. Instrum.* 13, P01025 (2018).

Synopsis

Low Gain Avalanche Detectors have been characterized using X-rays. Preliminary tests show promising results towards the development of soft X-ray single photon counting detectors.